Studies of spectral line merging in a laser-induced hydrogen plasma diagnosed with two-color Thomson scattering

Krzysztof Dzierżęga [*] and Franciszek Sobczuk[†]

Marian Smoluchowski Institute of Physics, Jagiellonian University, ul. Łojasiewicza 11, 30-348 Kraków, Poland

Evgeny Stambulchik [‡]

Faculty of Physics, Weizmann Institute of Science, Rehovot 7610001, Israel

Bartłomiej Pokrzywka [§]

Institute of Physics, Pedagogical University, ul. Podchorążych 2, 30-084 Kraków, Poland

Laser-induced hydrogen plasma in the density and temperature range of $(0.1–5) \times 10^{23}\,\mathrm{m}^{-3}$ and $(6000–20000)$ K, respectively, was precisely diagnosed using two-color Thomson scattering technique, inferring the electron number density, electron temperature as well as ion temperature. Simultaneously, spectra of the Balmer series of spectral lines from H-β to H-ζ were measured and plasma emission coefficient calculated within the quasicontiguous frequency-fluctuation model. The theoretical spectra are found to be in good agreement with experimental ones, including higher-density data where discrete lines were observed to merge forming a continuum.

I. INTRODUCTION

Modification of the atomic Coulomb potential due to the charged particles in the plasma environment decreases the energy of the bound states and makes the wave functions of higher excited levels delocalized [1], with the next charge state becoming energetically closer. This so-called continuum lowering or ionization potential depression (IPD) plays a key role in determining the ionization balance, charge-state distribution, opacity, and equation of state [2]. The unexpected IPD inferred in a recent study [3] has stirred intense discussion in the community, questioning the validity of widely used models [4,5]. In particular, it was argued that a completely consistent description must also take into account plasma fluctuations [6].

As with any other plasma phenomenon, IPD reveals itself through alteration of the radiative plasma properties and can be inferred by means of plasma spectroscopy [7]. Since some bound levels lose their "discrete" nature, so do the radiative transitions originating from these levels.

Indeed, the dynamic electric fields formed by the motion of charged plasma particles around a given atom perturb the atomic levels, causing not only the shift but also the broadening of the radiative transitions between them. This is commonly referred to as the plasma Stark broadening of spectral lines [8]. For a given set of plasma parameters, the effect

becomes more pronounced as the principal quantum number n increases, with the "discrete" spectral lines ultimately merging into a featureless continuum. Spectroscopically, this manifests itself as a shift of the continuum radiation (specifically, the free-bound one) towards lower energies. Therefore, both IPD and line merging manifest themselves via the disappearance of discrete higher-n transitions [9]. In general, care should be taken to distinguish between them. While IPD affects the ionization balance and thermodynamic plasma properties, the merging of the discrete transitions into continuum by itself does not.

The first successful treatment of line merging is due to Inglis and Teller [10], arguing that the discrete series merge into continuum when the Stark broadening of the higher level of transition equals to the energy separation between that level and the next one in the series. The eponymous Inglis-Teller limit defines the largest principal quantum number n_m of a hydrogenlike or Rydberg series at which the individual energy levels are sufficiently Stark broadened to merge with one another. Assuming the linear Stark effect, the width of the energy level is proportional to the product of the typical plasma microfield [11] $F_0 \propto N^{2/3}$, where N is the density of the charged particles, and the atomic dipole moment $d \propto n^2$ $(n \gg 1)$. With the energy separation between levels n and $n + 1$, $\Delta E_n \propto n^{-3}$, one obtains $n_m \propto N^{-2/15}$.

In general, both ions and electrons contribute to the Stark broadening, as already discussed in the original study [10]. There are certainly more issues to consider, especially at higher densities [12]. A crucial nontrivial assumption in the derivation of the limit is the linear Stark effect. Indeed, with n and/or N increasing, the size of the atomic orbitals $a_n \propto n^2$ approaches the interparticle distance $r_0 \propto N^{-1/3}$,

---

[*]Corresponding author: krzysztof.dzierzega@uj.edu.pl

[†]franciszek.sobczuk@doctoral.uj.edu.pl

[‡]Corresponding author: evgeny.stambulchik@weizmann.ac.il

[§]bartlomiej.pokrzywka@up.krakow.pl

causing nonlinear terms due to mixing of states with different n's and contribution of higher poles in the multipole expansion [13–15], field ionization [16–19], and penetrating collisions [20–22] to grow in importance. Equating a_n and r_0, one gets $n^* \propto N^{-1/6}$, and the same dependence follows from the field-ionization consideration, equating the classical ionization field $F_i \propto n^{-4}$ (e.g., Ref. [23]) and F_0. Note that $n^* \propto N^{-1/6}$ is quite close to the Inglis-Teller $n_m \propto N^{-2/15}$.

However, a refinement of the Inglis-Teller limit itself is not sufficient to accurately model the *entire* spectrum of a spectroscopic series, i.e., the shapes of the individual discrete lines and a smooth transition to the free-bound continuum, preserving the oscillator strength density [24]. Notably, the equivalence of analytical expressions for the oscillator strength of the bound-bound and free-bound radiation in hydrogen was pointed out by Menzel and Pekeris [25] long ago. There are various approaches to this problem, producing, in general, different results (e.g., see Refs. [24,26–31] and references therein).

Evidently, experimental spectra of an accurately diagnosed plasma can provide benchmark data for validating theoretical models. Although IPD and line merging are often discussed in the context of prominently transient [32] and degenerate [33] high-energy-density (HED) matter, the basic physics behind them is universal and can be investigated in moderate-density plasmas, with the advantage that precision diagnostics of such plasmas is less challenging. To this day, the emission measurements of the hydrogen Balmer series by Wiese *et al.* [34] remain the benchmark against which many theoretical calculations are compared. However, the electron density and temperature there were also obtained using emission data (based on the absolute line and continuum intensities), absolute line and continuum intensities. Moreover, no information was available on the temperature of the heavy particles. On the other hand, the ion temperature also affects the Stark broadening due to the ion dynamics [35] and ion coupling effects [36].

In this study, we present new experimental results regarding the Balmer series spectral lines and their transition to the continuum. Here, plasma properties were inferred independently of the emission spectra, based on the two-color Thomson scattering (TS) method [37], providing the electron density N_e and temperature T_e, and the ion temperature T_i in a single measurement. In spite of the fairly complex phenomena involved (described above), the measured spectra are shown to agree with the theoretical ones based on a simple semiempirical model with virtually no free parameters. This outcome adds credibility to the model to be considered for diagnostics of similar or even higher-energy-density plasmas, and provides an important insight for ab initio theoretical calculations yet to be developed.

II. THEORETICAL MODEL

A. Discrete lines

The shapes of individual lines are calculated within the quasicontiguous frequency-fluctuation model (QC-FFM) [38]. Briefly, the Stark pattern of a high-Δn H-like line between levels with the principal quantum number n and n' in the static electric field F can be represented by a rectangular shape within the quasicontiguous (QC) approximation [39]:

$$ I_{nn'}(\omega) = \begin{cases} \dfrac{I_{nn'}^{(0)}}{2\alpha_{nn'}F} & \text{for} \quad |\omega| \leqslant \alpha_{nn'}F, \\ 0 & \text{for} \quad |\omega| > \alpha_{nn'}F, \end{cases} \tag{1} $$

where $I_{nn'}^{(0)}$ is the total line intensity [40], and $\alpha_{nn'}$ is the linear-Stark-effect coefficient of the radiator with the core charge Z

$$ \alpha_{nn'} = \frac{3}{2Z}(n^2 - n'^2) \tag{2} $$

(throughout this section, atomic units are used, i.e., the electron mass m_e, the elementary charge e, the reduced Plank constant $\hbar$, and the Coulomb constant $1/(4\pi\epsilon_0)$ are all assumed unity).

Applying the frequency-fluctuation model (FFM) [41,42] to the QC approximation, the line shape broadened by a one-component plasma (OCP) is given by a universal functional [38]

$$ L(\bar{v}; \bar{\omega}) = \frac{1}{\pi} \Re \frac{J(\bar{v}; \bar{\omega})}{1 - \bar{v}J(\bar{v}; \bar{\omega})}, \tag{3} $$

with

$$ J(\bar{v}; \bar{\omega}) = \int_0^\infty d\tau \exp\left[-f(\tau) - i(\bar{\omega} - i\bar{v})\tau\right]. \tag{4} $$

Here, the area-normalized line shape L is expressed as a function of the dimensionless reduced detuning $\bar{\omega} = \omega/\Delta_0$ and $\bar{v}$, a single parameter related to the typical frequency of the microfields in the radiator-perturber center-of-mass frame [23]

$$ w_{\text{dyn}} = \sqrt{\frac{kT_p}{m_p} + \frac{kT_r}{m_r}} \left(\frac{4\pi N_p}{3}\right)^{1/3} \tag{5} $$

via

$$ \bar{v} = \frac{1}{2}\frac{w_{\text{dyn}}}{\Delta_0} + \frac{1}{20}\left(\frac{w_{\text{dyn}}}{\Delta_0}\right)^2, \tag{6} $$

where the second term is a semiempirical correction to recover the impact limit [8]. Z_p, N_p, m_p, and T_p are the charge, density, mass, and temperature of the OCP particles; m_r and T_r are the mass and temperature of the radiator. The normal detuning Δ_0 in several expressions above is defined as

$$ \Delta_0 = \alpha_{nn'}F_0, \tag{7} $$

where $F_0 = 2\pi(4/15)^{2/3}Z_p N_p^{2/3}$ is the Holtsmark normal field strength [11].

B. Microfield distribution

An essential ingredient of QC-FFM is $f(\tau)$ [see Eq. (4)], which is the characteristic function of the probability distribution of the plasma microfield magnitudes $\beta = F/F_0$

$$ W(\beta) = \frac{2}{\pi}\beta \int_0^\infty x \sin(\beta x)\exp\left[-f(x)\right]dx \tag{8} $$

(for an ideal plasma $f(x) = x^{3/2}$, corresponding to the Holtsmark distribution [11]). For a neutral radiator in a weakly coupled plasma, one seeks $f(x)$ in the form of $f(x) = x^{3/2}\psi_1(x)$ [43], with $\psi_1(x)$ conveniently expressed
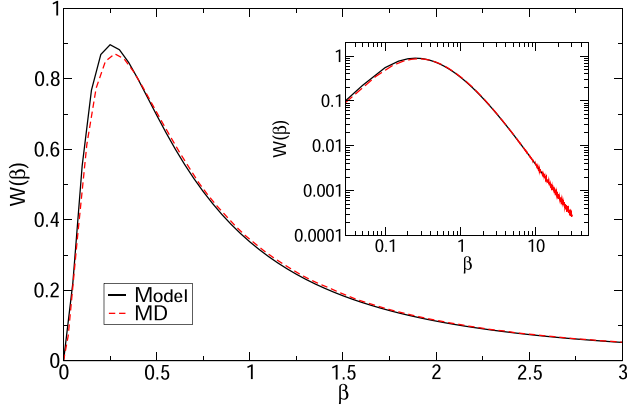
FIG. 1. Microfield distribution around a neutral radiator with the plasma coupling $\Gamma_p = 1.08$ assumed. Comparison of the analytical model using Eq. (11) with molecular dynamics (MD) simulations [45]. The same data are plotted in the log-log scale in the inset, showing the far tail of the distribution at larger values of β.

as a series of $v \propto \sqrt{\Gamma_p x}$ [44], where Γ_p is the coupling parameter:

$$\psi_1(x) = 1 + b_1 v + b_2 v^2 + \cdots . \qquad (9)$$

In fact, it was found that an inverse series

$$\psi_1(x) \approx 1/(1 + a_1 v + a_2 v^2), \qquad (10)$$

with $a_1 = -b_1$ and $a_2 = -b_2 + a_1^2$, has a wider convergence range while numerically evaluating Eq. (4). The actual expression used is

$$\psi_1(x) = 1/(1 + 1.295\sqrt{\Gamma_p x} + 0.606\,\Gamma_p x). \qquad (11)$$

In Fig. 1 we demonstrate that this approach reproduces the microfield distribution obtained using molecular-dynamics simulations [45] within 5% even for the rather significant plasma coupling on the order of unity. The agreement is much better for the lower values of plasma coupling that were attained in the experiment described here.

Equations (3), (4), and (11) give the shape of a discrete line due to a single plasma species (either electrons or ions). The total line shape is obtained by performing a convolution of the two.

C. Recombination continuum and the total spectrum

The calculations are carried out for the Balmer series going up in n until the Stark full width at half-maximum (FWHM) exceeds the distance to the next level (thus, similar in spirit to the Inglis-Teller considerations). The shape $L_{n_m}(\omega)$ of this last bound-bound transition is used to convolve with the free-bound (recombination) spectrum assumed to begin at ω_m placed right between the positions of the n_mth and $(n_m + 1)$th lines of the series. This approach is similar to the one described by Iglesias and Griem [46].

The free-bound intensity to level n ($n = 2$ for the Balmer series) is calculated using the Kramers's formula with the Gaunt-factor correction $g^{(n)}$:

$$I_{\text{rr}}(\omega) = \frac{8 Z^4 \alpha^3}{3\sqrt{3}\pi n^3} e^{-\omega/k_B T_e} g^{(n)} \equiv I_{\text{rr}}^{(0)} e^{-\omega/k_B T_e} . \qquad (12)$$

Here, $\alpha \approx 1/137$ is the fine-structure constant. In general, $g^{(n)}$ is a function of ω, but it varies only weakly around the recombination threshold [47]. For the present study, therefore, a constant value $g^{(2)} = 480\sqrt{3}\pi/e^8 \approx 0.8762$ [47] is used (note that e in the last expression is the base of the natural logarithm).

Thus, except for the thermodynamic Boltzmann factor, I_{rr} is a step function and its convolution with the Stark broadening function L_{n_m} is simply

$$I_{\text{rr}}(\omega) = I_{\text{rr}}^{(0)} \left[\frac{1}{2} + \int_0^{\omega - \omega_m} L_{n_m}(x) dx \right] \qquad (13)$$

(recall that L_{n_m} is area normalized by unity and note that the upper limit of the integral may be negative).

Finally, the total spectrum starting from H-β and up is

$$I(\omega) = \left[\omega^4 \sum_{n=4}^{n_m} \frac{I_n^{(0)}}{\omega_n^4} L_n(\omega) + I_{\text{rr}}(\omega) \right] e^{-\omega/k_B T_e} , \qquad (14)$$

where common, "trivial" $e^{-\omega/k_B T_e}$ and ω^4 dependences [48] are factored out [the latter only for the bound-bound transitions, since it is already implicitly included in $I_{\text{rr}}(\omega)$]. For brevity, the lower-level index $n' = 2$ was dropped in $I_{nn'}^{(0)}$ etc. Note that this expression assumes that all electron states—bound and free alike—are in the local thermodynamic equilibrium (LTE). This will be discussed in Sec. V.

III. EXPERIMENTAL SETUP

A simplified scheme of the experimental setup is presented in Fig. 2. A vacuum chamber was evacuated below 0.01 mbar and then filled with pure hydrogen at 1000 mbar. Plasma was created in the center of the chamber by focusing a second harmonic ($\lambda = 532$ nm) Q-switched Nd:YAG laser pulses (9.0 ns duration, 10 Hz repetition rate and 30 mJ) with an 75 mm focal length aspheric lens. The laser spots of about 46 μm in diameter resulted in a laser fluence of about 625 J/cm^2. All experimental parameters were matched to obtain shot to shot reproducible plasma plumes. For laser scattering experiments, a different, single-mode ($\delta\lambda < 0.5$ pm at 1064 nm, 6 ns duration, 10 Hz repetition rate) Nd:YAG laser was applied. Pulses generated from this laser were split into two, to pump the second and third harmonic generators. The resulting pulses of 532 nm and 355 nm were attenuated to energies of 1 mJ and 2 mJ, respectively, using Rochon prism polarizers and appropriate half-wave plates and then combined with a dichroic mirror. These probe laser beams, focused to spots of about 60 μm in diameter in the plasma volume, were propagating orthogonally to the pump, plasma generating one, and were polarized perpendicularly to the direction of observation. The delay between pump and probe pulses was controlled by a digital delay pulse generator with accuracy as good as 200 ps.

The plasma and laser-scattering (LS) light were observed perpendicularly to the laser beams by imaging the investigated area of plasma onto the entrance slit of a Czerny-Turner spectrometer (750 mm focal length, 0.502 nm/mm maximal reciprocal dispersion) with a magnification factor of 1.2. Plasma imaging was accomplished in the zeroth order of the spectrometer with a fully open entrance slit. Such imaging allowed for the verification of plasma reproducibility as well
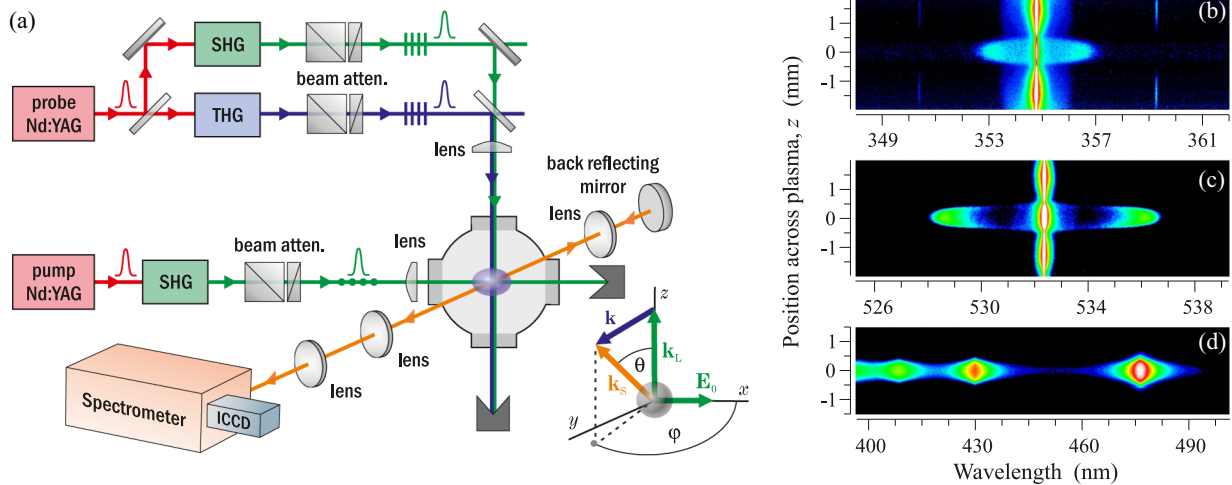
FIG. 2. Scheme of the experimental setup and the geometrical configuration of light beams (a), images of laser-scattering spectra at 355 nm (b) and 532 nm (c), and of plasma emission spectra (d) as recorded for a delay of 350 ns between the pump and probe laser pulses. The intensities of the optical signals are presented on a logarithmic scale. The white color in the images of the spectra does not mean the saturation of the ICCD, but only results from scaling the intensities in such a way that as much detail as possible of these spectra is noticeable.

as selecting the appropriate layer for further investigations. LS light and plasma emission spectra were recorded in the range from 6.65 nm to 106.4 nm (depending on the selected grating), with the entrance slit width being 50 μm and 20 μm, respectively. The instrumental profile, especially important for line profile measurements, was determined using different CW laser sources and is well approximated by the pseudo-Voigt function. The spectral sensitivity of the experimental optical and detection systems was determined using a calibrated halogen-deuterium lamp, while self-absorption of the studied spectral lines was verified with the back-reflecting mirror method [49]. This method consists in illuminating the plasma with its light reflected from a flat mirror placed behind the plasma column, at the opposite side to the spectrometer. An additional lens is placed between the mirror and the plasma in such a way that an image of the plasma is formed on the mirror surface. When reflected back, it coincides with the original plasma plume. Comparing the spectra recorded with and without the back mirror, the global reflectance spectrum of the mirror can be determined, which is related to the absorption spectrum of the plasma.

Optical signals were recorded with a gated two-dimensional intensified charge-coupled device (ICCD) camera mounted in the focal plane of the spectrometer. The ICCD was synchronized to the pump and probe pulses in case of emission and LS measurements, respectively. To improve the signal-to-noise ratio of TS spectra, the ICCD gate width was as short as 9 ns. Subsequently, emission signals were recorded with the gate width set to about 3% of the respective delay time between the pump and probe laser pulses, e.g., at 15 ns for a 500 ns delay, to probe quasistationary plasma. The emission and LS spectra were averaged over 10000 and 50000 laser shots, respectively, and were studied in the time interval (time delay) from 60 ns to 700 ns after the pump pulse. A very large number of averages in the case of TS measurements was due to very low energy of the probe pulses to avoid potential plasma heating in the inverse bremsstrahlung process.

Images of LS and plasma emission spectra, recorded in the experiment for a delay of 350 ns, are shown in Fig. 2. These spectra are already corrected for the dark current of the CCD matrix and the spectral sensitivity of the experimental system. It should be emphasized that the presented LS spectra are of high spatial resolution, limited only by the size of the probe laser beams in the interaction area, while the emission spectra are integrated along the observation direction and require further processing, i.e., inverse Abel transformation to recover the radially resolved spectra, corresponding to LS ones. These two LS spectra are composed of two distinct sidebands corresponding to the electron feature of Thomson scattering and indicate here the partially collective character of the TS process. Moreover, a decrease in their shifts and widths, as we move away from the center of the plasma, indicates a rapid decrease in the electron density and electron temperature. Much stronger central parts of these spectra, at the wavelengths of the probe lasers, include both the ionic feature of TS and the Rayleigh scattering signals.

IV. RESULTS

A. Plasma diagnostics by two-color Thomson scattering

For hydrogen plasma diagnostics, we applied the two-color laser Thomson scattering (2CTS) method [37]. Compared to the single-wavelength TS, 2CTS also provides information about the ionic temperature apart from the electron temperature and the electron density. Unlike emission methods, TS is generally free of assumptions about the thermodynamic equilibrium of plasma and its chemical composition, and the results are characterized by high spatial resolution in all directions. The single-wavelength TS method has recently been used for plasma diagnostics in studies aimed at verifying the calculations of the Stark profiles of the He [50], Li [51], and Ar [52] spectral lines. In turn, Tomita *et al.* [53] and Crintea *et al.* [54] used TS for comparative studies of plasma diagnostics obtained with newly developed emission methods applied for blasted arcs and inductively coupled plasmas, respectively.

In TS, the power scattered about the scattering angle θ (see Fig. 2) and within the frequency range $d\omega$ as a function of the frequency shift $\omega = \omega_s - \omega_L$ is given by

$$\frac{dP_T(\omega)}{d\Omega}d\omega = \eta P_L L \Delta\Omega \, N_e \frac{d\sigma_T}{d\Omega} S_T(\mathbf{k}, \omega) \, d\omega, \qquad (15)$$

where η is the wavelength dependent efficiency of the optical and detection systems, P_L is the average power of the incident laser beam, L the length of the scattering volume, and $\Delta\Omega$ the detection solid angle. Furthermore, N_e is the electron number density while $d\sigma_T/d\Omega = r_e^2(1 - \sin^2\theta\cos^2\varphi)$ is the differential cross section for the Thomson scattering of an electromagnetic wave by a free electron with r_e classical electron radius. The spectral distribution of the scattered photons is described by the spectral density function $S_T(\mathbf{k}, \omega)$ depending on the scattering geometry, laser wavelength, and plasma properties. For plasmas with Maxwellian velocity distribution, the spectral density function, under the Salpeter approximation can be written as [55,56]

$$
\begin{aligned}
S_T(\mathbf{k}, \omega) \, d\omega &= S_e(\mathbf{k}, \omega) \, d\omega + S_i(\mathbf{k}, \omega) \, d\omega \\
&\approx \left| \frac{1}{1 + \alpha^2 W(x_e)} \right|^2 \frac{\exp\left(-x_e^2\right)}{\sqrt{\pi}} dx_e \\
&\quad + Z\alpha^4 \left| \frac{1}{1 + \alpha^2 + \alpha^2 Z(T_e/T_i)W(x_i)} \right|^2 \\
&\quad \times \frac{\exp\left(-x_i^2\right)}{\sqrt{\pi}} dx_i.
\end{aligned}
\qquad (16)
$$

Here, $x_e = \omega/(kv_e)$ and $x_i = \omega/(kv_i)$, where $v_{e,i} = \sqrt{(2k_B T_{e,i}/m_{e,i})}$ is the thermal mean velocity of electrons (e) or ions (i), Z is the charge number of the ion while $W(x)$ is the plasma dispersion function. The scattering parameter

$$\alpha \equiv 1/(k\lambda_D) = \frac{\lambda_L}{4\pi \sin(\theta/2)} \sqrt{\frac{N_e e^2}{\varepsilon_0 \, k_B T_e}} \qquad (17)$$

with λ_D, electron Debye length and λ_L, laser wavelength. The scattering wave vector $\mathbf{k} = \mathbf{k}_s - \mathbf{k}_L$, where $\mathbf{k}_L$ and $\mathbf{k}_s$ are the wave vectors of the incident laser beam and the observed scattered light, respectively. Two terms of Eq. (16), after Salpeter are called, the electron and ion features and their spectra take on different shapes depending on α.

In order to determine the electron number density and electron temperature, the electron parts of the two TS spectra (recorded successively for laser wavelengths of 355 nm and 532 nm), originating from a specific region of the plasma and for a fixed delay, were simultaneously fitted by the resulting spectral density function that is, the convolution of the appropriate spectral density functions with the apparatus one

$$\tilde{S}_e(\omega) \equiv [(S_e(\mathbf{k}_L = \mathbf{k}_{355}) + S_e(\mathbf{k}_L = \mathbf{k}_{532})) * f](\omega). \quad (18)$$

The results of fitting to the corresponding TS spectra for the on-axis ($z = 0.0$ mm) plasma and for the delay of 180 ns, are presented in Fig. 3.

The total, frequency integrated, amplitude of the spectral density function of TS spectrum is expressed
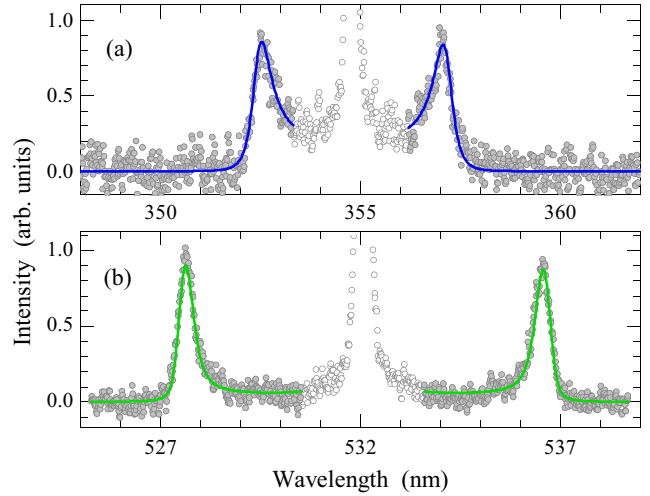
FIG. 3. TS spectra recorded at a delay of 180 ns on the plasma axis ($z = 0$) for two probe lasers of (a) 355 nm and (b) 532 nm. Solid lines represent curves fitted with the resultant spectral density function [Eq. (18)] while full circles are fitted data as corresponding to the electron part of the TS spectrum. The electron number density and electron temperature determined this way are 1.903×10^{23} m^{-3} and 16020 K, respectively.

as [56]

$$
\begin{aligned}
S_T(\mathbf{k}) &\equiv \int S_T(\mathbf{k}, \omega) d\omega = S_e(\mathbf{k}) + S_i(\mathbf{k}) \\
&= \frac{1}{1 + \alpha^2} + \frac{Z\alpha^4}{(1 + \alpha^2)[1 + \alpha^2(1 + ZT_e/T_i)]}.
\end{aligned}
\qquad (19)
$$

Its ion part directly depends on the T_e/T_i ratio, which is used to measure the ion temperature provided N_e and T_e are already known. The amplitude of S_T particularly strongly varies with T_e/T_i for $\alpha \gtrsim 1$, i.e., for at least partially collective scattering, which is the case of our plasma conditions under study.

The ion component of TS occurs in the central part of the scattering spectrum (at wavelength of the probe laser) and is two orders of magnitude narrower than the electron one [57]. Therefore, these two components are in principle easily distinguishable and separable. However, the very small spectral width of the ion component and its overlap with the Rayleigh scattering (RS) signal, which inherently accompanies TS, is a major experimental challenge. To separate TS and RS contributions, and then to determine the ion temperature, we applied the 2CTS method using two probe lasers of significantly different wavelengths and leveraging the wavelength dependence of the RS and TS signal cross sections [37].

2CTS plasma diagnostics can be explained as follows. For a given wavelength of the probe beam, the ratio of the total power of LS in plasma to LS in the reference medium (H$_2$ gas at 294 K room temperature and 1000 mbar pressure) is

$$
\begin{aligned}
R_\lambda &\equiv \frac{dP_T/d\Omega + dP_R/d\Omega}{dP_{H_2}/d\Omega} \\
&= \left(\frac{N_e}{N_{H_2}}\right)\left(\frac{d\sigma_{H_2}(\lambda)}{d\Omega}\right)^{-1}\left(\frac{d\sigma_T}{d\Omega}\right)[S_e(\mathbf{k}) + S_i(\mathbf{k}, T_e/T_i)] \\
&\quad + \left(\frac{N_H}{N_{H_2}}\right)\left(\frac{d\sigma_{H_2}(\lambda)}{d\Omega}\right)^{-1}\bar{\sigma}_\Omega(\lambda).
\end{aligned}
\qquad (20)
$$

TABLE I. Parameters of 2CTS configuration and physical constants applied and used in our experiment and calculations.

Probe laser wavelengths, λ_L	355 nm and 532 nm
scattering angles, $\theta = \varphi$	90°
differential TS cross section, $d\sigma_T/d\Omega$	7.941×10^{-30} m²/sr
differential RS cross section on Ar [58],	
$d\sigma_{Ar}/d\Omega$ (355 nm)	2.86×10^{-31} m²/sr
$d\sigma_{Ar}/d\Omega$ (532 nm)	5.46×10^{-32} m²/sr
differential RS cross section on H_2[a]	
$d\sigma_{H_2}/d\Omega$ (355 nm)	7.21×10^{-32} m²/sr
$d\sigma_{H_2}/d\Omega$ (532 nm)	1.33×10^{-32} m²/sr
number density of H_2 molecules	
at reference conditions, N_{H_2}	2.463×10^{25} m⁻³

[a]Values determined in this work by measuring and comparing the respective Rayleigh scattering signals for hydrogen and argon.

In the Rayleigh scattering process, assuming Knudsen regime with LS spectra of the Gaussian type, the total power scattered by atoms and/or molecules into the solid angle $d\Omega$ is given by

$$\frac{dP_R(\lambda)}{d\Omega} = \eta P_L L \Delta\Omega \sum_j n_j \bar{\sigma}_{\Omega,j}(\lambda), \qquad (21)$$

where n_j is the number density of specific particles while $\bar{\sigma}_{\Omega,j}$ is the effective differential cross section for scattering on these particles in a given direction, and is defined as

$$\bar{\sigma}_{\Omega,j}(\lambda) \equiv \sum_k q_{j,k} \frac{d\sigma_{j,k}(\lambda)}{d\Omega}. \qquad (22)$$

In the above equation, $q_{j,k}$ denotes the fraction of the jth species in their kth state, while $d\sigma_{j,k}/d\Omega$ is the corresponding Rayleigh differential cross section. In the investigated hydrogen plasma, only hydrogen atoms in their ground and excited states significantly contribute to the RS signal.

Based on the predetermined electron number density and temperature, and by measuring the relative scattering signals R_λ for two probe laser beams, the solution of the system of two equations of the form of Eq. (20) yields T_i and the magnitude of the Rayleigh contribution measured by the product $N_H \cdot \bar{\sigma}_{\Omega,j}$. All physical constants and experimental parameters used in our calculations are collected in Table I. In this work, the required differential cross sections for Rayleigh scattering on the reference molecular hydrogen gas were determined against the corresponding differential cross sections for argon given by Thalman *et al.* [58]. For this purpose, the respective Rayleigh scattering signals were recorded and then compared.

The results of plasma diagnostics by 2CTS method show a homogeneous distribution of its parameters (N_e, T_e, and T_i) in the near-axis area with a radius of about 0.2 mm. For studies on hydrogen plasma emission spectra, only this central, homogeneous part of the plasma column was further considered.

The uncertainties of the derived plasma parameters were evaluated based on the statistical uncertainties of the fitted spectral density function [Eq. (18)] and on the total intensities of TS and RS spectra. In the case of our transient plasma, the electron number density is subject to larger fluctuations than the electron temperature due to its larger spatial gradient and faster decay [57,59]. The final values of the plasma

TABLE II. Plasma parameters as derived using 2CTS method for plasma axis and at various delays between the pump and the probe laser beams. Experimental results include upper and lower limits of their maximal uncertainties.

Delay (ns)	α(532 nm)	N_e (10^{23} m⁻³)	T_e (K)	T_i (K)
60	4.180	$4.548^{+0.142}_{-0.052}$	19590^{+330}_{-250}	19300^{+1500}_{-1400}
180	2.990	$1.903^{+0.084}_{-0.060}$	16020^{+270}_{-230}	15300^{+1500}_{-1400}
350	2.283	$0.977^{+0.067}_{-0.078}$	14110^{+500}_{-550}	15500^{+2800}_{-2800}
500	1.957	$0.543^{+0.015}_{-0.028}$	10670^{+300}_{-440}	6800^{+780}_{-970}
600	1.637	$0.273^{+0.013}_{-0.025}$	7680^{+540}_{-740}	5030^{+860}_{-1100}
700	1.224	$0.118^{+0.019}_{-0.027}$	5900^{+270}_{-520}	3200^{+2000}_{-2300}

parameters, obtained for the plasma axis and for the considered delays, along with their uncertainties, are presented in Table II.

B. Plasma emission spectra

Images of laterally integrated emission spectra of hydrogen plasma were first corrected for the dark current of the ICCD and smoothed using the Savitzky–Golay filtering. By applying the procedure described in Ref. [49] no evidence was found indicating clear self-absorption of the investigated spectral lines. It was inferred based on the reflectance coefficient of the back mirror, which showed no wavelength dependence in the investigated spectral range in contrast to the H-α region. This line undergoes quite significant self-absorption, especially at shorter delays, i.e., in hotter plasma with higher electron density. Therefore, all investigated spectra were treated as originating from an optically thin medium. Radially resolved spectra were then retrieved applying the inverse Abel transformation [59,60] and only those coming from the central (near axis) homogeneous zone of the plasma column were further considered. The resulting spectra contain the Balmer series hydrogen lines as well as continuum plasma radiation and are shown in Fig. 4.

The figure also shows the theoretical spectra calculated for the plasma parameters as derived using the 2CTS method and then convolved with instrumental profiles. The theoretical spectra were augmented by adding a background linearly dependent on the wavelength. This background approximates a sum of all sources of continuum radiation except for the Balmer recombination spectrum, which is explicitly included in Eq. (14). The two parameters of the background function as well as the total scaling factor were varied to minimize χ^2 while superimposing the experimental and theoretical spectra.

V. DISCUSSION

Except for the 700-ns delay case that is discussed below, the calculations reproduce the measured spectra very well, in particular, the phenomenon of line merging below the Balmer limit. The only statistically significant disagreements between the measured and calculated spectra are seen in the central part of H-β. However, this is expected. The QC approximation [39] is derived assuming $\Delta n \gg 1$, which, among the transitions measured, is least justified in the case of H-β ($\Delta n = 2$).
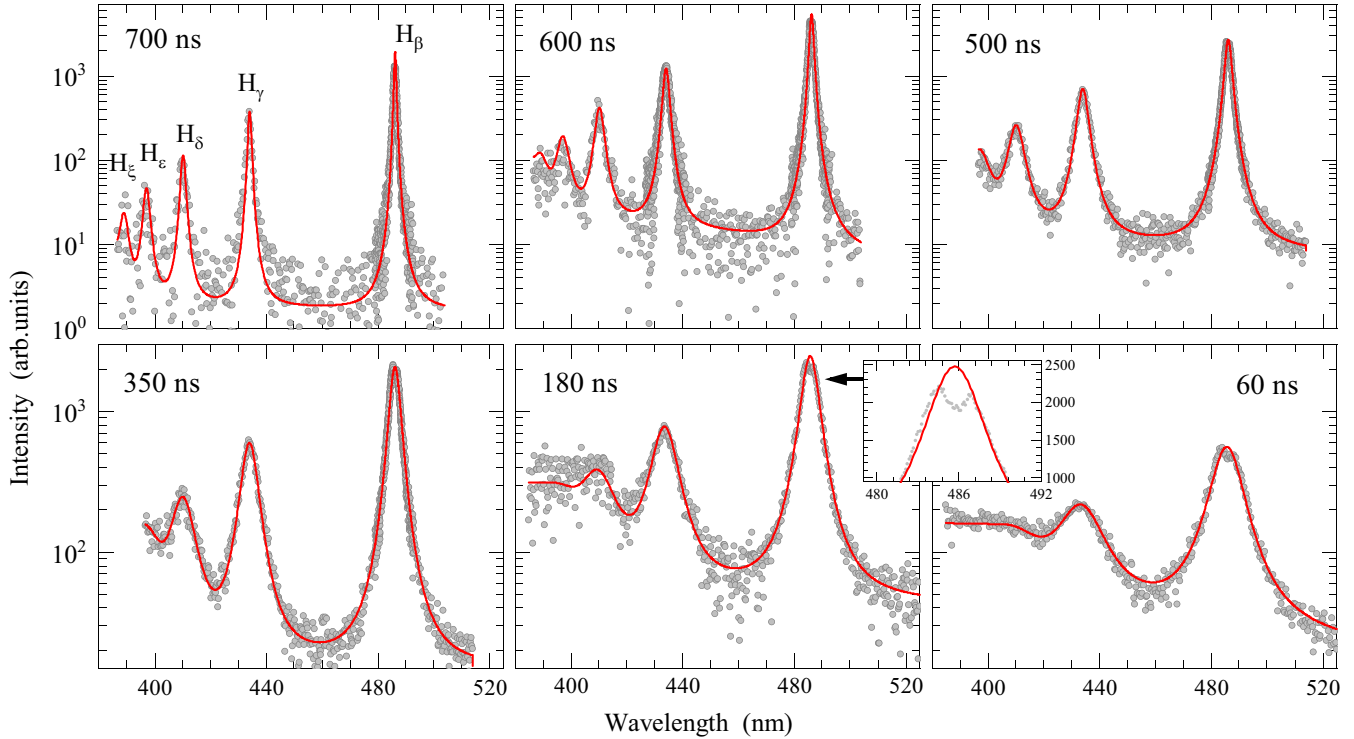
FIG. 4. Experimental (dots) and theoretical (lines) spectra of the hydrogen Balmer series as observed and calculated at different time delays of the laser-induced plasma in hydrogen at pressure of 1000 mbar .

In particular, QC cannot by definition reproduce the central dip in the Stark profile of this line. The measured H-β shapes do feature the familiar two-peak structure (see the inset at 180 ns) with a noticeable asymmetry at higher densities due to the nonlinear Stark effect (e.g., see Refs. [13,14]). A detailed analysis of individual lower-n transitions will be given elsewhere [37].

As already mentioned, in the spectra calculated using Eq. (14), LTE level populations were assumed. For the hydrogen plasma with the electron temperature on the order of 1 eV as in the present study, this implies the electron density in excess of 10^{23} m^{-3} (e.g., see Eq. (7.75) in Ref. [7]). However, even for lower densities the *relative* populations of the excited bound levels as well as the ionized charge state are very well described by the Boltzmann exponent, i.e., they are in the partial LTE. This is demonstrated in Fig. 5, where the ratios of the level populations in a collision-radiative equilibrium [61] to their respective LTE values are shown. Therefore, although in absolute units Eq. (14) is not always justified, multiplying it by a constant factor to fit the experimental results (as done in the present study) is.

Another assumption made is the thermal equilibrium between hydrogen atoms and protons, i.e., $T_r = T_i$. An equilibrium of this type is much more likely than between ions and electrons due to the much greater energy exchange in a single atom-proton collision than in the atom-electron one. Nevertheless, it is possible that the temperature of neutral hydrogen differs from that of protons due to the incomplete thermalization of the plasma. This would affect the line broadening due to the Doppler and Stark effects, the latter through the microfield frequency, Eq. (5). However, these two possible

minor inaccuracies also partially cancel out. For example, $T_r < T_i$ would yield a smaller Doppler broadening (which is anyway small compared to the Stark width), while the lower microfield frequency would result in a small increase of the Stark broadening of high-n transitions [38]. The total uncertainty in the line widths due to the incomplete equilibrium of the heavy particles is estimated to be $\lesssim 2\%$ under the whole range of the experimental conditions.

The minor but systematic differences between the calculated and measured line widths in the 700-ns case are attributed to the influence of neutral perturbers. The plasma at
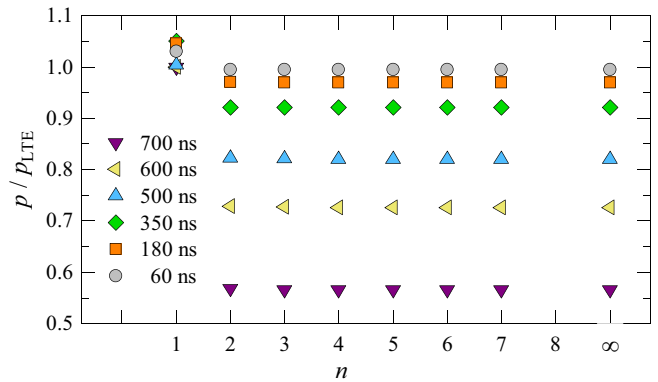
FIG. 5. Steady-state level populations relative to the LTE values for plasma conditions inferred in the experiment at different time delays (given in the legend). For clarity, bound levels up to $n = 7$ are shown. The rightmost data points in each series correspond to the bare nucleus.
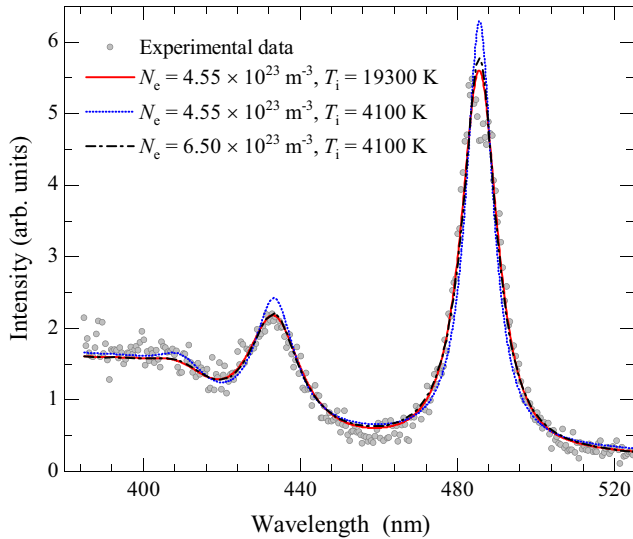
FIG. 6. Experimental (dots) and theoretical (lines) spectra of the hydrogen Balmer series as observed and calculated for the 60-ns case. The effect of varying the ion temperature and the electron number density with constant $T_e = 19590$ K is demonstrated (see Sec. V).

such a long delay is very weakly ionized, and, therefore, the growing importance of the neutrals becomes noticeable. Although, as mentioned above, the properties of neutral species were not investigated in the present work, their effect on the line profile can be estimated. Assuming that the density and temperature of the neutral hydrogen in the plasma correspond to the initial gas density and T_i, respectively, the sum of the resonance and Van der Waals broadenings (e.g., see Chap. 4.8 of Ref. [7]) is consistent with the observed discrepancies within a factor of two.

In the present study, the difference between T_e and T_i turned out to be moderate or none within the uncertainty limits when the density was high and hence, the continuum lowering most pronounced. However, this was not obvious *a priori*. In fact, in many HED plasmas determining T_i is a highly challenging task undertaken because of its crucial importance [62]. To demonstrate the possible inaccuracy that may result from a wrongly determined T_i, in Fig. 6 we show a calculated spectrum assuming a hypothetical value of T_i, which is significantly lower than the experimentally inferred one at the delay of 60 ns . In this case, the agreement with the measured spectrum is evidently worse—measured by as much as the 150% increase in the value of the reduced χ^2. This effect is mostly due to the smaller line broadening. To

compensate for this narrowing and restore the goodness of the fit, one would need to assume a higher $N_e \approx 6.5 \times 10^{23}$ m^{-3}, which is 40% above the real value.

VI. SUMMARY AND CONCLUSIONS

We have presented experimental and theoretical studies of the Balmer series line spectra and their merging into continuum in laser-induced hydrogen plasma of moderate electron number density in the range from 10^{22} m^{-3} to 5×10^{23} m^{-3}.

The plasma was diagnosed by the two-color Thomson scattering method, independently of emission spectra and free of assumptions about the plasma equilibrium. The inferred electron number density, electron temperature, as well as the ion temperature are spatially and time resolved. Simultaneously, plasma spectra were recorded, and their spatial distributions were retrieved using the inverse Abel transformation procedure.

The line-shape calculations in the discrete-spectrum domain were performed within the quasicontiguous frequency-fluctuation model, carried out until the Stark FWHM exceeded the distance to the next level. Plasma electrons and ions were treated on an equal footing in the model. The recombination spectrum was analytically continued towards the respective lower energy and convolved with the shape of the last discrete transition, resulting in the total spectrum that preserves the oscillator strength density. The experimental and theoretical spectra are found to be in good agreement, including the region where the discrete lines and the continuum emission merge.

We believe that the experimental data, including very reliable plasma parameters, may serve as the benchmark against which theoretical calculations are compared, similarly to the data presented by Wiese *et al.* [34]. We also believe that the same calculational approach can be applied to model the spectra of hydrogenlike ions or Rydberg series of any species, providing efficient density diagnostic of laboratory and space plasmas.

ACKNOWLEDGMENTS

[1] R. M. More, Pressure ionization, resonances, and the continuity of bound and free states, in *Advances in Atomic and Molecular Physics*, edited by D. R. Bates and B. Bederson (Academic Press, New York, 1985), Vol. 21, pp. 305–356.

[2] B. J. B. Crowley, Continuum lowering – A new perspective, High Energy Density Phys. **13**, 84 (2014).

[3] O. Ciricosta, S. M. Vinko, H.-K. Chung, B.-I. Cho, C. R. D. Brown, T. Burian, J. Chalupský, K. Engelhorn, R. W. Falcone, C. Graves, V. Hájková, A. Higginbotham, L. Juha, J. Krzywinski, H. J. Lee, M. Messerschmidt, C. D. Murphy, Y. Ping, D. S. Rackstraw, A. Scherz, W. Schlotter, S. Toleikis, J. J. Turner, L. Vysin, T. Wang, B. Wu, U. Zastrau, D. Zhu,

R. W. Lee, P. Heimann, B. Nagler, and J. S. Wark, Direct Measurements of the Ionization Potential Depression in a Dense Plasma, Phys. Rev. Lett. **109**, 065002 (2012).

[4] G. Ecker and W. Kröll, Lowering of the ionization energy for a plasma in thermodynamic equilibrium, Phys. Fluids **6**, 62 (1963).

[5] J. C. Stewart and K. D. Pyatt, Lowering of ionization potentials in plasmas, Astrophys. J. **144**, 1203 (1966).

[6] C. A. Iglesias and P. A. Sterne, Fluctuations and the ionization potential in dense plasmas, High Energy Density Phys. **9**, 103 (2013).

[7] H. R. Griem, *Principles of Plasma Spectroscopy* (Cambridge University Press, Cambridge, England, 1997).

[8] H. R. Griem, *Spectral Line Broadening by Plasmas* (Academic, New York, 1974).

[9] M. Nantel, G. Ma, S. Gu, C. Y. Côté, J. Itatani, and D. Umstadter, Pressure Ionization and Line Merging in Strongly Coupled Plasmas Produced By 100-fs Laser Pulses, Phys. Rev. Lett. **80**, 4442 (1998).

[10] D. R. Inglis and E. Teller, Ionic depression of series limits in one-electron spectra, Astrophys. J. **90**, 439 (1939).

[11] J. Holtsmark, Über die Verbreitung von Spektrallinien, Ann. Phys. (Leipzig) **363**, 577 (1919).

[12] S. Alexiou, Scaling of hydrogen electron Stark widths at high densities and the Inglis–Teller limit, High Energy Density Phys. **5**, 68 (2009).

[13] S. Djurović, M. Ćirišan, A. V. Demura, G. V. Demchenko, D. Nikolić, M. A. Gigosos, and M. Á. González, Measurements of H$_\beta$ Stark central asymmetry and its analysis through standard theory and computer simulations, Phys. Rev. E **79**, 046402 (2009).

[14] T. A. Gomez, T. Nagayama, D. P. Kilcrease, M. H. Montgomery, and D. E. Winget, Effect of higher-order multipole moments on the Stark line shape, Phys. Rev. A **94**, 022501 (2016).

[15] A. V. Demura, Beyond the linear Stark effect: A retrospective, Atoms **6**, 33 (2018).

[16] D. G. Hummer and D. Mihalas, The equation of state for stellar envelopes. I - an occupation probability formalism for the truncation of internal partition functions, Astrophys. J. **331**, 794 (1988).

[17] D. V. Fisher and Y. Maron, Effective statistical weights of bound states in plasmas, Eur. Phys. J. D **18**, 93 (2002).

[18] A. Calisti, L. A. Bureyeva, V. S. Lisitsa, D. Shuvaev, and B. Talin, Coupling and ionization effects on hydrogen spectral line shapes in dense plasmas, Eur. Phys. J. D **42**, 387 (2007).

[19] P.-E. Tremblay, P. Bergeron, J. S. Kalirai, and A. Gianninas, New insights into the problem of the surface gravity distribution of cool DA white dwarfs, Astrophys. J. **712**, 1345 (2010).

[20] S. Alexiou, R. W. Lee, S. H. Glenzer, and J. I. Castor, Analysis of discrepancies between quantal and semiclassical calculations of electron impact broadening in plasmas, J. Quant. Spectrosc. Radiat. Transfer **65**, 15 (2000).

[21] J.-C. Pain and F. Gilleron, Modeling penetrating collisions in the standard line broadening impact theory for hydrogen, High Energy Density Phys. **30**, 52 (2019).

[22] C. A. Iglesias, Penetrating collisions in hydrogen spectral line broadening by plasmas, High Energy Density Phys. **35**, 100743 (2020).

[23] E. Stambulchik and Y. Maron, Plasma formulary interactive, J. Instrum. **6**, P10009 (2011).

[24] L. G. D'yachkov, Smooth transition from spectral lines to a continuum in dense hydrogen plasma, High Temp. **54**, 5 (2016).

[25] D. H. Menzel, C. L. Pekeris, and H. Shapley, Absorption coefficients and hydrogen line intensities, Mon. Not. R. Astron. Soc. **96**, 77 (1935).

[26] W. Dappen, L. Anderson, and D. Mihalas, Statistical mechanics of partially ionized stellar plasma: The Planck–Larkin partition function, polarization shifts, and simulations of optical spectra, Astrophys. J. **319**, 195 (1987).

[27] F. J. Rogers and C. A. Iglesias, Radiative atomic Rosseland mean opacity tables, Astrophys. J. Supp. Ser. **79**, 507 (1992).

[28] P.-E. Tremblay and P. Bergeron, Spectroscopic analysis of DA white dwarfs: Stark broadening of hydrogen lines including nonideal effects, Astrophys. J. **696**, 1755 (2009).

[29] C. Lin, G. Röpke, H. Reinholz, and W.-D. Kraeft, Ionization potential depression and optical spectra in a Debye plasma model, Contrib. Plasma Phys. **57**, 518 (2017).

[30] S. Alexiou, E. Stambulchik, T. Gomez, and M. Koubiti, The fourth workshop on lineshape code comparison: line merging, Atoms **6**, 13 (2018).

[31] R. R. Sheeba, M. Koubiti, Y. Marandet, T. Qbaich, J. Rosato, and R. Stamm, Modeling of line and continuum spectral emission of hydrogen for recombining plasma conditions, J. Phys. Conf. Ser. **1289**, 012041 (2019).

[32] R. Jin, M. M. Abdullah, Z. Jurek, R. Santra, and S.-K. Son, Transient ionization potential depression in nonthermal dense plasmas at high x-ray intensity, Phys. Rev. E **103**, 023203 (2021).

[33] G. Röpke, D. Blaschke, T. Döppner, C. Lin, W.-D. Kraeft, R. Redmer, and H. Reinholz, Ionization potential depression and Pauli blocking in degenerate plasmas at extreme densities, Phys. Rev. E **99**, 033201 (2019).

[34] W. L. Wiese, D. E. Kelleher, and D. R. Paquette, Detailed study of the Stark broadening of Balmer lines in a high-density plasma, Phys. Rev. A **6**, 1132 (1972).

[35] S. Ferri, A. Calisti, C. Mossé, J. Rosato, B. Talin, S. Alexiou, M. A. Gigosos, M. Á. González, D. González-Herrero, N. Lara, T. Gomez, C. A. Iglesias, S. Lorenzen, R. C. Mancini, and E. Stambulchik, Ion dynamics effect on Stark broadened line shapes: A cross comparison of various models, Atoms **2**, 299 (2014).

[36] D. Alumot, E. Kroupp, E. Stambulchik, A. Starobinets, I. Uschmann, and Y. Maron, Determination of the Ion Temperature in a High-Energy-Density Plasma Using the Stark Effect, Phys. Rev. Lett. **122**, 095001 (2019).

[37] F. Sobczuk, K. Dzierżęga, and E. Stambulchik (unpublished).

[38] E. Stambulchik and Y. Maron, Quasicontiguous frequency-fluctuation model for calculation of hydrogen and hydrogenlike Stark-broadened line shapes in plasmas, Phys. Rev. E **87**, 053108 (2013).

[39] E. Stambulchik and Y. Maron, Stark effect of high-n hydrogenlike transitions: quasi-contiguous approximation, J. Phys. B: At. Mol. Opt. Phys. **41**, 095703 (2008).

[40] L. McLean, General expression for intensity of hydrogen lines, Nature (London) **129**, 25 (1932); General expression for the intensity of hydrogen lines, Phil. Mag. **18**, 845 (1934).

[41] B. Talin, A. Calisti, L. Godbert, R. Stamm, R. W. Lee, and L. Klein, Frequency-fluctuation model for line-shape calculations in plasma spectroscopy, Phys. Rev. A **51**, 1918 (1995).

[42] A. Calisti, C. Mossé, S. Ferri, B. Talin, F. Rosmej, L. A. Bureyeva, and V. S. Lisitsa, Dynamic Stark broadening as the Dicke narrowing effect, Phys. Rev. E **81**, 016406 (2010); L. A. Bureeva, M. B. Kadomtsev, M. G. Levashova, V. S. Lisitsa, A. Calisti, B. Talin, and F. Rosmej, Equivalence of the method of the kinetic equation and the fluctuating-frequency method in the theory of the broadening of spectral lines, JETP Lett. **90**, 647 (2010).

[43] B. Mozer and M. Baranger, Electric field distributions in an ionized gas. II, Phys. Rev. **118**, 626 (1960).

[44] H. Pfennig and E. Trefftz, Die Druckverbreiterung der diffusen Heliumlinien, Vergleich zwischen Messung und Theorie im quasistatischen Bereich, Z. Naturforsch. A **21**, 697 (1966).

[45] E. Stambulchik and Y. Maron, A study of ion-dynamics and correlation effects for spectral line broadening in plasma: K-shell lines, J. Quant. Spectrosc. Radiat. Transfer **99**, 730 (2006).

[46] E. J. Iglesias and H. R. Griem, Transparency window effect in the Inglis–Teller region of the BV Lyman series, J. Quant. Spectrosc. Radiat. Transfer **55**, 383 (1996).

[47] I. A. Kotelnikov and A. I. Milstein, Electron radiative recombination with a hydrogen-like ion, Phys. Scr. **94**, 055403 (2019).

[48] H. R. Griem, Theory of wing broadening of the hydrogen Lyman-α line by electrons and ions in a plasma, Phys. Rev. **140**, A1140 (1965).

[49] M. Cvejić, M. Gavrilović, S. Jovićević, and N. Konjević, Stark broadening of Mg I and Mg II spectral lines and Debye shielding effect in laser induced plasma, Spectrochim. Acta Part B **85**, 20 (2013).

[50] E. Nedanovska, G. Nersisyan, T. Morgan, L. Hüwel, C. L. S. Lewis, D. Riley, and W. Graham, Comparison of the electron density measurements using Thomson scattering and emission spectroscopy for laser induced breakdown in one atmosphere of helium, Appl. Phys. Lett. **99**, 261504 (2011).

[51] K. Dzierże\!¸ga, T. Pie\!¸ta, W. Zawadzki, E. Stambulchik, M. Gavrilović-Bozović, S. Jovanović, and B. Pokrzywka, Study of Stark broadening of Li I 460 and 497 nm spectral lines with

independent plasma diagnostics by Thomson scattering, Plasma Sources Sci. Technol. **27**, 025013 (2018).

[52] K. Dzierżęga, W. Zawadzki, F. Sobczuk, M. L. Sankhe, S. Pellerin, M. Wartel, W. Olchawa, A. Bacławski, and A. Bartecka, Experimental and theoretical studies of Stark profiles of Ar I 696.5 nm spectral line in laser-induced plasma, J. Quant. Spectrosc. Radiat. Transfer **237**, 106635 (2019).

[53] K. Tomita, D. Gojima, T. Shimizu, K. Uchino, T. Nakano, Y. Tanaka, K. Suzuki, T. Iijima, and T. Shinakai, Thomson scattering diagnostics of sf_6 gas-blasted arcs confined by a nozzle unedr free-recovery conditions, J. Phys. D: Appl. Phys. **48**, 265201 (2015).

[54] D. L. Crintea, U. Czarnetzki, S. Iordanova, I. Koleva, and D. Luggenholscher, Plasma diagnostics by optical emission spectroscopy on argon and comparison with Thomson scattering, J. Phys. D: Appl. Phys. **42**, 045208 (2009).

[55] E. E. Salpeter, Electron density fluctuations in a plasma, Phys. Rev. **120**, 1528 (1960).

[56] O. E. Evans and J. Katzenstein, Laser light scattering in laboratory plasmas, Rep. Prog. Phys. **32**, 207 (1969).

[57] K. Dzierżęga, A. Mendys, and B. Pokrzywka, What can we learn about laser-induced plasmas from Thomson scattering experiments, Spectrochim. Acta Part B **98**, 76 (2014).

[58] R. Thalman, K. J. Zarzana, M. A. Tolbert, and R. Volkamer, Rayleigh scattering cross-section measurements of nitrogen, argon, oxygen and air, J. Quant. Spectrosc. Radiat. Transfer **147**, 171 (2014).

[59] T. J. Pięta, Comparative studies of laser-induced plasma using optical emission spectroscopy and laser Thomson sattering, Ph.D. thesis, Jagiellonian University, Kraków, 2020.

[60] S. L. Montgomery, D. R. Keefer, and S. I. Sudharsanan, Abel inversion using transform techniques, J. Quant. Spectrosc. Radiat. Transfer **39**, 367 (1988).

[61] E. Stambulchik and Y. Maron, CRaC: A collisional-radiative code for dense plasmas (unpublished).

[62] Y. Maron, Experimental determination of the thermal, turbulent, and rotational ion motion and magnetic field profiles in imploding plasmas, Phys. Plasmas **27**, 060901 (2020).